DOI: 10.13009/EUCASS2023-576
Aerospace Europe Conference 2023 – 10TH EUCASS – 9TH CEAS

From short to too-short arcs: admissible states region theory and boundary use for surveillance observations

Laura Pirovano[1†] *and Matteo Losacco*[2] *and Roberto Armellin*[1] *and Carlos Yanez* [3] *and Emmanuel Delande* [3] *and* Stéphanie Lizy-Destrez[2]

[1]*Te Pūnaha Ātea - Space Institute, University of Auckland, 20 Symonds Street, 1010, Auckland, New Zealand*
[2]*Institut Supérieur de l'Aéronautique et de l'Espace (ISAE-SUPAERO), 10 Av. Edouard Belin, 31400 Toulouse, France*
[3]*Centre National d'Études Spatiales (CNES), 18 Av. Edouard Belin, 31400, Toulouse, France*

laura.pirovano@auckland.ac.nz
[†]Corresponding author

Abstract

This work develops a rigorous metric for the identification of the boundary between the short and the too-short arcs regimes in the initial orbit determination process. The proposed approach makes use of differential algebra and domain-splitting techniques to investigate the presence of singularities in the formulation of the initial orbit determination process. When these are detected, a six-dimensional reformulation of the classical admissible region concept is employed. Examples for ground and space-based sensor types are then presented.

1. Introduction

Space Situational awareness tasks require an accurate estimation of the state of objects orbiting around the Earth. These estimates are derived from networks of ground-based and space-based optical, radar, and laser sensors that operate all over the world to continuously monitor the near-Earth environment. This surveillance action, however, currently covers just a very small portion of the resident space objects (RSO) population whose size is continuously growing due to the unrelenting launch activity, coupled with in-orbit object generation events, such as collisions, fragmentations and explosions.[1] As a result, observation campaigns often offer the possibility of identifying uncatalogued objects. Due to their surveillance nature, however, these campaigns can only record short streaks, which can be as long as the sensor field of view, at best.

The process of state estimation of an uncatalogued object starting from a set of measurements is known in the literature as initial orbit determination (IOD). Such measurements are typically referred to as tracks, or tracklets. Three families of IOD algorithms exist, i.e. classical angle-only and angle-range methods for optical and range radars respectively,[2] and recent angle-Doppler methods for range rate radars.[3,4] Whenever the process is successful, the tracklet is usually referred to as a short arc. Conversely, if the available observations are too close in time and the noise levels are too high to perform IOD, the passage is referred to as a too-short arc and shall be processed by relying on different approaches, e.g. the admissible region (AR) theory.[5] Surveillance observations often lie on the boundary between short and too-short arcs.

We highlight two current limitations in the available state estimation theory:

1. for a successful IOD process, the solution is usually given in the form of a point solution, relying on literature methods such as Gauss, Lambert, or Gooding among others. Hence, there is a lack of information on the estimated uncertainty. The estimation of the solution uncertainty is, however, essential to establish robust data association schemes enabling catalog initialization;

2. a clear boundary between the short and the too-short arcs regimes does not exist, i.e. metrics to a priori determine whether the collected observations provide enough information to obtain a robust IOD solution, or AR-based

DOI: 10.13009/EUCASS2023-576

approaches shall be followed, are not available. The metric shall employ as input both the tracklets length and the precision of the observations, to determine whether both the state and its uncertainty can be estimated, in accordance with point 1.

To overcome the first limitation, new methods based on the use of Differential Algebra (DA)[6] have been presented in the last five years. DA-based reformulations of the IOD problem, called Differential Algebra Initial Orbit Determination (DAIOD) methods, were recently presented for range radars,[7] optical sensors,[8] and Doppler radars,[9] whereas a six-dimensional extension of the AR concept, called admissible states region (ASR), has been recently formulated for optical observations.[10]

The DAIOD output is called the Orbit Set (OS), which is the analytical representation of all states fitting through three observations depending on the precision of the observations. Figure 1 shows an artistic representation of the OS as the shaded green area and blue lines, which is the geometrical solution of all ellipses fitting through the black observational arc with a precision specified by the red circles.

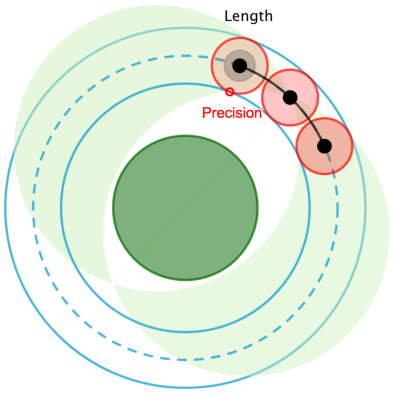

Figure 1: Artistic impression of the OS.

Regarding the second limitation, it is possible to empirically delineate the boundary between IOD and AR approaches by looking at the success rate of the DAIOD algorithm, as in Fig. 2. From this plot one can understand whether a point solution and its uncertainty can be defined from a short arc of defined length and precision, that is whether the shaded green area and blue lines of Fig. 1 are fully defined analytically.

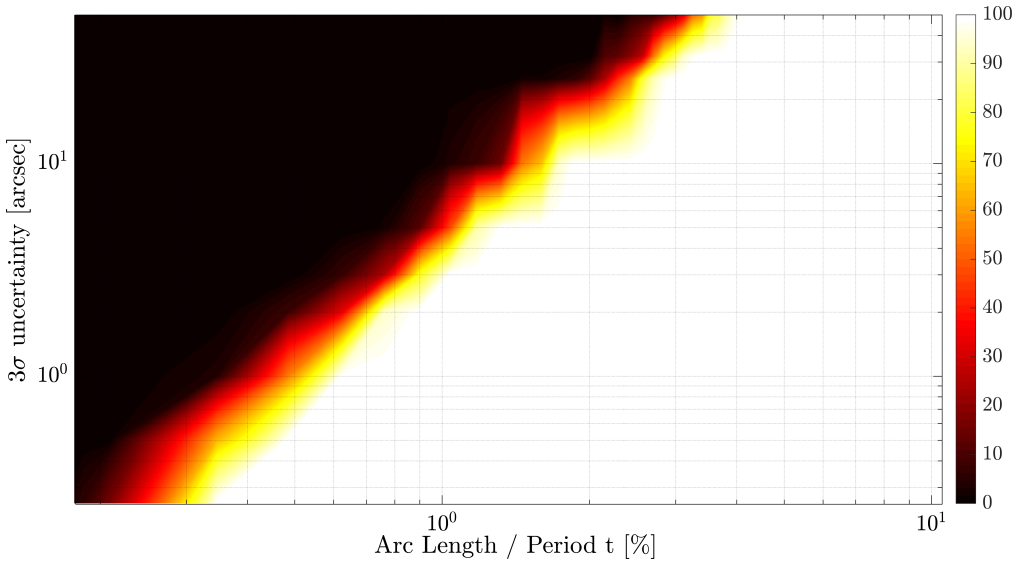

Figure 2: OS success rate for optical observation of a geostationary Earth orbit (GEO) object depending on tracklet length and observation precision [Taken from Pirovano et al.[8]].

Only a previous work by Dichter[11] attempted to define an indicator for the success of the IOD, but it could only establish whether a point solution was obtainable. Starting from the described DA-based estimation methods, Section 2 develops a metric for identifying the boundary between the short and too-short arcs regimes, for the definition of both a point solution and its uncertainty, meaning it describes a rigorous mathematical procedure to determine the pattern observed in Fig. 2. The resulting method is from now on referred to as Determinant Singularity Detection (DSD) algorithm. Section 3 then illustrates the basic concepts of the ASR theory, improves the current methodology to obtain a smaller uncertainty region, and extends it to all sensor types.

DOI: 10.13009/EUCASS2023-576

2. The Determinant Singularity Detection (DSD) approach

The present work aims at describing a methodology that works for observations regardless of the sensor type or the observatory location. For this reason, Table 1 summarises the minimal observation set, observable and unobservable spaces for different sensor types, to then enunciate a unified methodology for all cases. The angular information is expressed in terms of receiver topocentric right ascension α and declination δ and their time derivatives, whereas ρ and $\dot{\rho}$ indicate the topocentric range and range rate, respectively. Optical sensors provide two values of angles per time instant. Measurement regression can be then exploited to obtain an estimate of their time derivatives, whereas no information about ρ and $\dot{\rho}$ is available. Range-only radars offer an additional information, as they provide for each observation epoch the value of the object slant range d, i.e. the sum of the distances of the transiting object from the receiver and the transmitter. By knowing the angular position of the object, the value of ρ can be easily retrieved. Doppler-only radars, instead, couple the angular information with the time derivative of the slant range, $\dot{d}$. This value then coincides, apart from a scaling factor, with $\dot{\rho}$ in case of monostatic radar, while this no longer holds for bistatic radars.

Table 1: Sensor types, minimal observation set, observable and unobservable space for surveillance observations.

Sensor type	Min # observations	Observable space $\boldsymbol{O}$	Unobservable space $\overline{\boldsymbol{O}}$
Optical	3	(α, δ)	$(\dot{\alpha}, \dot{\delta}, \rho, \dot{\rho})$
Range-only Radar	2	(α, δ, ρ)	$(\dot{\alpha}, \dot{\delta}, \dot{\rho})$
Doppler-only Radar	3	(α, δ)	$(\dot{\alpha}, \dot{\delta}, \rho, \dot{\rho})$

Starting from the work developed for optical observations,[8] we have extended the OS theory to all sensor types, adapting the algorithm to the different observable spaces.[9] All methods share the same building blocks, or a subset of thereof, to obtain the initial point solution:

- Gauss method is used to provide an estimate of the ranges when ranges are not observable;
- Once ranges are available, either via Gauss or the observable space, Lambert arcs are used to make sure that the orbit found is an ellipse that passes through the two or three observation points.

Reference 9 also introduced a further step to reduce the failing rate of the Gauss algorithm, by searching for a candidate point solution in the entire uncertain observable space, rather than just in the raw measurements, while Reference 8 introduced observables regression to reduce the influence of noise. Once the canditate state $\boldsymbol{X_O}$ is available, the observables are "augmented" with their uncertainty in polynomial form:

$$[\boldsymbol{O}] = \boldsymbol{O} + \boldsymbol{CI_O} \cdot \boldsymbol{x}; \quad \boldsymbol{x} \in [-1, 1]^N,$$

where the brackets $[\cdot]$ represent a variable in polynomial form, N is the size of the observable $\boldsymbol{O}$, whereas $\boldsymbol{CI_O}$ are the confidence intervals derived from either the standard deviations of raw measurements or the regression process. This process is performed within the DA framework. Once the initialization is computed, every function evaluation performed with a DA variable returns the Taylor expansion of the evaluated function. This means that the expansion point is the typical numerical function evaluation and the polynomial expansion describes the sensitivity of the function to the DA input. By evaluating the augmented set $[\boldsymbol{O}]$ in the function developed to obtain $\boldsymbol{X_O}$, a Taylor expansion around the candidate solution is found depending on the observables precision:

$$[\boldsymbol{X_O}] = \boldsymbol{X_O} + \mathcal{T}_{\boldsymbol{X}}(\boldsymbol{x}).$$

$[\boldsymbol{X_O}]$ is the so-called OS. A more in-depth description of the methods can be found in Reference 8 and 9.

It is a specific step in this procedure that prompted the current research. To obtain the polynomial expansion $\mathcal{T}$, the following Jacobian was calculated and then inverted:

$$[J] = \frac{\partial \boldsymbol{Y}}{\partial \overline{\boldsymbol{O}}} = \mathcal{T}_J(\boldsymbol{O}),$$

where $\boldsymbol{Y}$ is a function of the state to be calculated, and the function is specific to the sensor considered. The inversion is successful if and only if the determinant of the Jacobian is non-zero. A singularity in the determinant would instead prevent the solution to be found on the entire observable space $[\boldsymbol{O}]$. The calculation of the determinant of the Jacobian

DOI: 10.13009/EUCASS2023-576

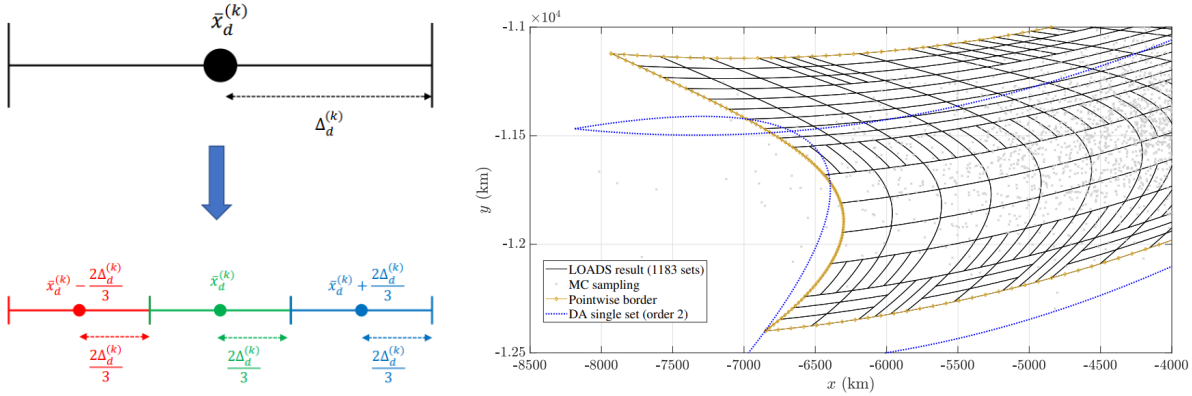

(a) (b)

Figure 3: (a) LOADS technique splitting the domain into three equal sub-domains to keep an accurate low-order representation of the domain. The dots represent the centers of the Taylor expansions, where the middle one preserves the original expansion point. (b) shows an example of the use of the LOADS. The blue dots represent the uncertainty region without truncation error control, the gold dots are the pointwise computation of the uncertainty borders, and the grey dots are the Montecarlo simulation. In contrast, the LOADS automatically detects such borders accurately and splits the domain accordingly to keep the uncertainty representation accurate in polynomial form. [Taken from Losacco et al.[12]]

is thus the detection tool we need to discern between a short arc and a too-short arc, hence its name: Determinant Singularity Detection (DSD) approach.

Approximating generic non-linear functions with polynomials does not ensure accuracy on the entire [$\boldsymbol{O}$] domain. In order to keep the polynomial expansion accurate, we use the low order automatic domain splitting (LOADS) algorithm.[12] The LOADS takes care of the truncation error of polynomial expansions over a set domain. If the error exceeds a threshold, the domain is split over three new equally divided domains. The procedure continues until the truncation error is below the threshold in each sub-domain. As a result, a quasi-linear description of the Taylor expansion of the determinant is obtained.

Once the determinant of the Jacobian is described in polynomial form over a finite number of sub-domains, polynomial bounding techniques are then applied to estimate the minimum and maximum value of the determinant over each sub-domain. Discordant signs over the extremes imply the presence of a singularity. This technique removes the need for sampling, thus avoiding computational expensive Montecarlo simulations while allowing a thorough search for singularities on the entire uncertainty domain. In case no singularity is detected, the IOD problem is well posed, thus DAIOD methods can be applied. Otherwise, the ASR theory shall be employed. Figure 3 shows the basic principle of the LOADS and an application to highlight its features: accurate representation of the uncertainty region and automatic splitting of the uncertainty domain without the need for Montecarlo sampling.

3. The Admissible State Region (ASR) theory

When the DSD triggers a singularity warning, the classical IOD methods fail in describing the uncertain observation as an OS. The AR[13] approach is then preferred. As previously introduced, we have developed a DA-based counterpart called the ASR for optical observation, and will now extend it to different sensor types. The original AR is built by imposing energetic constraints to define the limits on the non-observed quantities, while the observable space is regressed in the so-called attributable $\mathcal{A}$. The AR coincides with the object range ρ and its time derivative $\dot{\rho}$ for an optical observation, while, for example, collapses to the range only in the case of monostatic Doppler radar. The AR thus bounds the unobservable space $\overline{\boldsymbol{O}}$. In our DA implementation, the unobservable space $\overline{\boldsymbol{O}}$ is enclosed in a rectangle as in Fig. 4a, hence wrapping around the AR constraints, and the attributable is equipped with a confidence interval derived from the student-T distribution[10] to account for the uncertainty of the observations, hence reaching the six-dimensional uncertainty definition of the ASR.

DOI: 10.13009/EUCASS2023-576

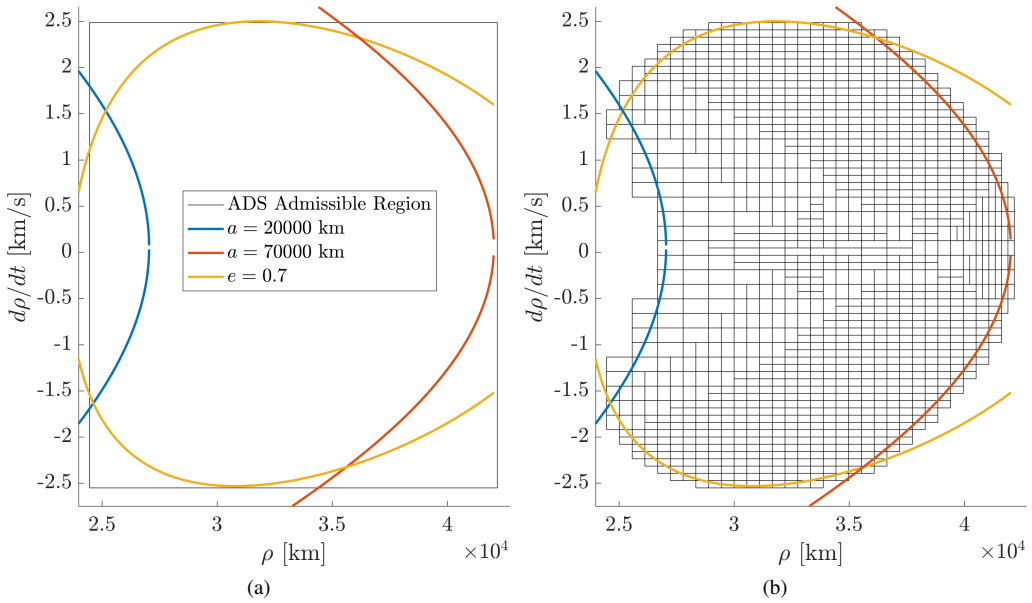

Figure 4: ASR for an optical observation in GEO, before (a) and after (b) the first pruning. [Taken from Pirovano et al.[10]]

Given the AR and the associated observation uncertainty, the second step consists in identifying a proper enclosure of the AR, to be handled within the DA framework, since the box identified in Fig. 4a includes a rather large useless area. The idea is to be able to describe the analytical bounds of the AR through Taylor polynomials and the automatic domain splitting (ADS),[14] which is the high-order counterpart of the LOADS. To do so, two consecutive pruning actions are performed. The first pruning action exploits the conversion from polar to Keplerian parameters. The polar coordinates are fully available in DA thanks to the box enclosure of the unobservable space and the regression of the observable space within the attributable. By converting such six-dimensonal region into Keplerian elements, the ADS is triggered and sub-domains are created. The resulting sub-domains of Keplerian parameters then pass through a polynomial bounder, and only those that are compliant with the expected limits are retained. An example is shown in Fig. 4, where the initial ASR encloses the analytical constraints - Fig. 4a - and through the transformation and pruning Fig. 4b is obtained.

The first pruning provides a better discretization of the AR, but does not offer any means to distinguish between the different solutions, that is any point in the domain is equally probable at this point. To exploit all possible information contained in a tracklet, and to improve the initial description of the ASR presented in Pirovano et al.,[10] the second step considers the raw observations. Each identified sub-domain contains the analytical description of the state $[\boldsymbol{X}]$, meaning that also the predicted observables $\hat{\boldsymbol{O}}$ relative to each sub-domain can be computed as Taylor expansions:

$$[\hat{\boldsymbol{O}}] = f(\boldsymbol{X}) = \mathcal{T}_{\hat{\boldsymbol{O}}}(\boldsymbol{O}, \overline{\boldsymbol{O}})$$

Assuming that each observation in a tracklet can be treated as an independent identically distributed Gaussian variable, it is possible to construct a χ^2 test to check whether each sub-domain or part of thereof is probabilistically compatible with the real observations. The sum of the N standardized observation residuals square on the sub-domain k is:

$$[r_k] = \sum_{i=1}^{N} \frac{(\boldsymbol{O}_i - [\hat{\boldsymbol{O}}]_{i,k})^2}{\sigma_i^2}.$$

and behaves as a $\chi^2(M)$, where $M = o \cdot n$ are the degrees of freedom, o is the number of measurements per instant and n the number of time instants. The test aims at finding if the predicted observations match the real ones by looking for residuals that fall below the threshold set by $\mathrm{CDF}^{-1}_{\chi^2(M)}(\alpha)$, where α is the confidence level. More specifically, for each resulting residual map, a polynomial bounder is used to have a first estimate of the value of the minimum residual. If this estimate is below the imposed threshold, a polynomial solver is used to compute the real minimum of the residual expansion over its domain. If this minimum is again below the imposed threshold, then the set is considered compliant with the available measurements, and it is retained, otherwise, it is discarded. This second pruning aims at reducing the

DOI: 10.13009/EUCASS2023-576

size of the uncertainty region of the ASR to improve the efficiency of data association tools. This is especially useful for those tracklets that fall on the boundary of the feasibility of the IOD algorithm, where thus a simple regression into the attributable may reduce the amount of information extracted. The use of raw data past the initial filter thus aims at recovering the potentially lost data.

4. Results

4.1 The DSD

In this section, optical observations are simulated to understand the evolution of the determinant bound size depending on the tracklet observation and precision. Then, the performance of the DSD is compared against Fig. 2.

Figure 5a shows the evolution of the determinant bounds for increasing length and uncertainty of simulated tracklets. For the plot, 293 objects in low Earth orbit (LEO) were simulated from 5 different ground-based observatories. Tracklets lengths spanned from 30 to 420 s, and precision varied from 1 to 10 arcsec. For long tracklets, the bar plot shows how the length of the observation dominates over the precision in terms of determinant bounds. For shorter observations, instead, both the length and the precision are incisive in the bounds sizes. This is understandable, as for a long tracklet the curvature of the resulting orbit is well defined and can only be slightly changed by observation uncertainty. For shorter tracklets, as underlined in Fig. 1, both circular and highly elliptical orbits can fit in the observations, hence a reduction in the arc length and/or an increase in uncertainty have a similar effect on the determinant bound size.

The second result here presented concerns the comparison between the empirically defined boundary in Fig. 2 and the newly defined analytical DSD. Figure 5b shows a section of Fig. 2 around an arc length 1% of the object period (a GEO object) and the DSD results on the right-hand side for different precision spanning from $3\sigma = 0.25$ arcsec to $3\sigma = 50$ arcsec. By inflating the uncertainty for a given arc length, we expect the determinant bounds to increase in size, as experienced in Fig. 5a. This time, the sign of the bounds is of interest. When both the lower and upper bound of the determinant are positive, the problem is well-posed and the DAIOD algorithm can be used to solve the IOD. As soon as the lower bound becomes negative, there exists at least one point in the observation uncertainty that cannot be mapped into a feasible state. Hence, the ASR approach needs to be used. The DSD step only takes 0.1 s to determine whether the tracklet is a short arc or a too-short arc. As can be seen in Fig. 5b, the DSD is triggered for $3\sigma > 6$ arcsec for the case at hand. The empirical bound is placed between 3 and 7 arcsec, following a Montecarlo simulation, hence resulting compatible with the newly designed metric.

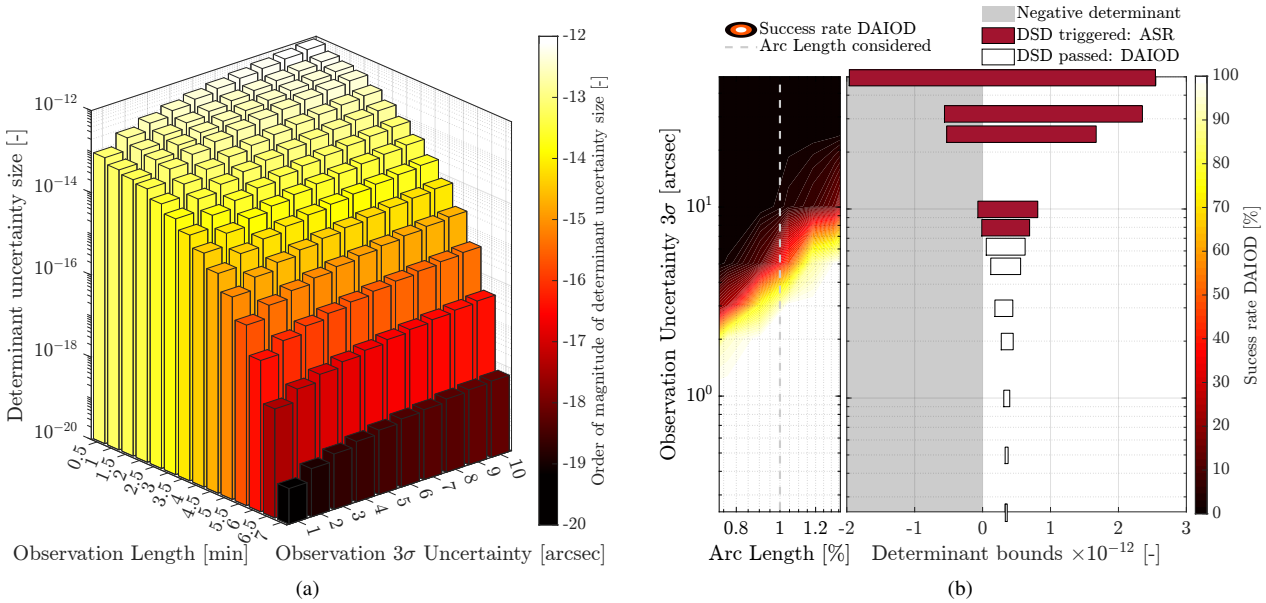

Figure 5: (a) Analysis on the estimated size of the uncertainty of the Jacobian determinant depending on arc length and observation uncertainty. (b) Comparison between a section of Fig.2 and the determinant bounds for one observation of a GEO object corresponding to an arc length of 1% of the object period.

DOI: 10.13009/EUCASS2023-576

4.2 The ASR

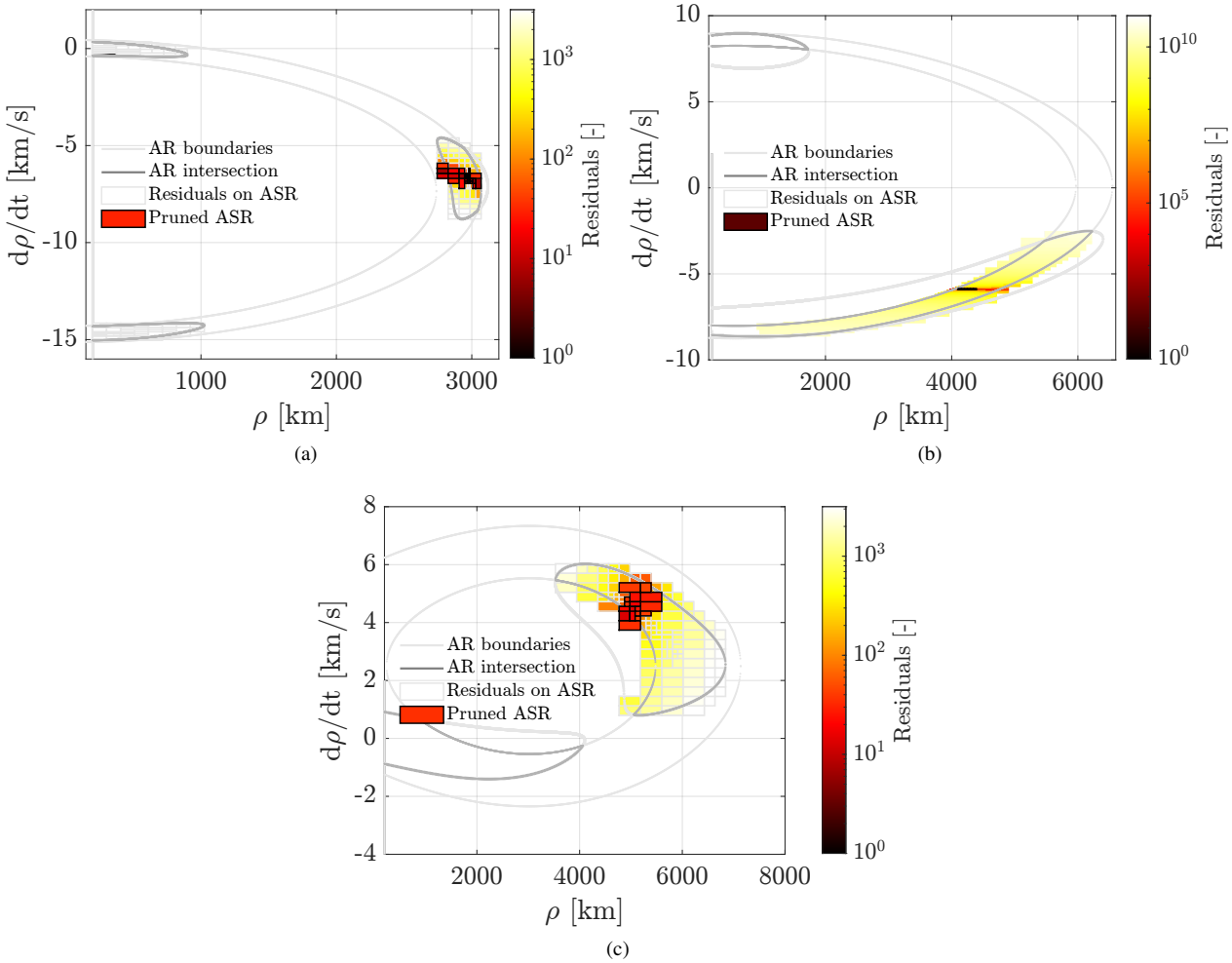

Figure 6: Admissible states regions for a ground-based optical telescope (a) and a bistatic Doppler radar (b) and a space-based optical sensor (c) when targeting a LEO object. The light grey lines represents the classical AR, the grey boxes the result of the first pruning action, whereas the coloured boxes refer to the minimum residuals. Sets retained at the end of the second pruning are enclosed in black boxes.

The two-step pruning approach previously described is here presented on a set of ground and space-based optical and radar measurements. This is the first time the ASR is extended to sensor types other than ground-based optical observatories. Figure 6a shows the ASR generated when observing a LEO object with a ground-based optical sensor. The light grey lines represent the classical AR, i.e. define the admissible regions identified by constraints on the minimum and maximum semi-major axis values and on the maximum eccentricity. The grey boxes are the result of the first pruning action, whereas the coloured boxes refer to the minimum residuals. Sets retained at the end of the second pruning are enclosed in black boxes. Three disconnected regions can be identified, namely two regions located at low ρ values and a third one located almost at the boundaries of the a_{max} admissible region. The presence of multiple regions is made possible by the threshold imposed for the maximum eccentricity e_{max}. As this value increases, the two regions of the left of the plot increase in size. All the regions are accurately discretized by the first pruning action, which however is not capable of identifying where the real state of the observed object lies. This selection is performed by the residuals-based pruning action, which automatically eliminates the two regions on the left and significantly shrinks the size of the remaining one.

The size of the resulting pruned admissible regions strongly depends on the imposed confidence level for the χ^2 distribution, the measurement noise level, and the number of measurements per time instant. As the confidence level increases, the threshold for the inverse of the cumulative distribution increases, thus more sets are likely to be retained after the pruning action. The measurement noise levels, instead, enter at the denominator of the residuals formula.

DOI: 10.13009/EUCASS2023-576

As a result, for a given passage, the higher the noise, the larger the expected size of the retained ASR. The number of measurements per time instant, instead, plays a twofold role, as a larger value causes the both the residuals level and the CDF threshold to increase. Overall, sensor like Doppler-only radars that couple the angular position of the object with an additional information are likely to generate a smaller ASR (see Fig. 6b). Figure 6c shows the ASR when targeting a LEO object from an observer located on a circular polar orbit with 1000 km of altitude. No uncertainty on the location of the observer is considered. Space-based optical observations provide the same level of information of their ground-based counterpart, but are characterized by a faster relative motion between target and observer. This generates a motley set of admissible regions, which in number and shape can significantly differ from typical ground-based cases, as shown in Fig. 6c.

5. Conclusions

The paper introduced a new analytical metric to discern between short arcs and too-short arcs, such that the appropriate algorithm can be used to perform initial orbit determination (IOD) and obtain the associated state estimate and its uncertainty. The metric revolves around the calculation of the determinant of a Jacobian involved in the definition of the state estimation. Since the inverse of the Jacobian is sought, the determinant must be positive. By applying Differential Algebra (DA) techniques, the determinant of the Jacobian is found as a Taylor expansion of the observation uncertainty. Determinant singularities are thus treated as polynomial root searches. Thanks to the efficient polynomial bounder enabled by the DA description of the determinant, the computational intensive Montecarlo sampling is not necessary to obtain information about the singularities. The so-called Determinant Singularity Detection (DSD) is able to determine whether the tracklet is a short arc (no singularities) or a too-short arc (singularities) in a fraction of a second, such that the appropriate technique can be used to extract as much information as possible from the tracklet, respectively the Differential Algebra Initial Orbit Determination (DAIOD) algorithm or the admissible states region (ASR) algorithm. The latter is treated in this paper and its definition is extended to all types of surveillance scenarios: ground- and space-based observations for optical, radar and doppler radar sensors.

Acknowledgements

Dr Pirovano's and Dr Armellin's work was supported by AOARD under Grant FA2386-21-1-4115. Dr Losacco's work is founded by CNES through the R-S20/BS-0005-058 and R-S22/BS-0005-058 grants.

References

[1] ESA Space Debris Office, "ESA's Annual Space Environment Report," techreport, European Space Agency, May 2021.

[2] J. C. Dolado, C. Yanez, and A. Anton, "On the performance analysis of Initial Orbit Determination algorithms," *Proc. 67th IAC*, 2016.

[3] C. Yanez, F. Mercier, and J. Dolado Perez, "A novel initial orbit determination algorithm from Doppler and angular observations," *Proc. 7th European Conference on Space Debris*, 2017.

[4] J. A. Christian and W. E. Parker, "Initial Orbit Determination from Bearing and Range-Rate Measurements Using the Orbital Hodograph," *Journal of Guidance, Control, and Dynamics*, Vol. 44, No. 2, 2021, pp. 370–378, 10.2514/1.G005433.

[5] D. Farnocchia, G. Tommei, A. Milani, and A. Rossi, "Innovative methods of correlation and orbit determination for space debris," *Celestial Mechanics and Dynamical Astronomy*, Vol. 107, 2010, pp. 169–185, 10.1007/s10569-010-9274-6.

[6] M. Valli, R. Armellin, P. Di Lizia, and M. Lavagna, "Nonlinear Mapping of Uncertainties in Celestial Mechanics," *Journal of Guidance, Control, and Dynamics*, Vol. 36, No. 1, 2013, pp. 48–63, 10.2514/1.58068.

[7] R. Armellin and P. Di Lizia, "Probabilistic Optical and Radar Initial Orbit Determination," *Journal of Guidance, Control, and Dynamics*, Vol. 41, No. 1, 2018, pp. 101–118, 10.2514/1.G002217.

[8] L. Pirovano, D. A. Santeramo, R. Armellin, P. Di Lizia, and A. Wittig, "Probabilistic data association: the orbit set," *Celestial Mechanics and Dynamical Astronomy*, Vol. 132, No. 15, 2020, 10.1007/s10569-020-9951-z.

DOI: 10.13009/EUCASS2023-576

[9] M. Losacco, R. Armellin, C. Yanez, S. Lizy-Destrez, L. Pirovano, and F. Sanfedino, "Robust Initial Orbit Determination for Surveillance Doppler-Only Radars," *IEEE Transactions on Aerospace and Electronic Systems*, 2023, 10.2514/1.G004866.

[10] L. Pirovano, R. Armellin, J. Siminski, and T. Flohrer, "Differential algebra enabled multi-target tracking for too-short arcs," *Acta astronautica*, Vol. 182, 2021, pp. 310–324, 10.1016/j.actaastro.2021.02.023.

[11] M. J. Dichter and J. J. Wojcik, "Characterizing the Convergence Behavior of Gauss's Method of Initial Orbit Determination," *Journal of Guidance, Control, and Dynamics*, Vol. 43, No. 5, 2020, pp. 998–1002, 10.2514/1.G004866.

[12] M. Losacco, A. Fossà, and R. Armellin, "A low-order automatic domain splitting approach for nonlinear uncertainty mapping," *preprint submitted to the Journal of Guidance, Control, and Dynamics*, Unpublished results, pp. 1–42, http://arxiv.org/abs/2303.05791.

[13] K. J. DeMars, M. K. Jah, and P. W. Schumacher, "Initial Orbit Determination using Short-Arc Angle and Angle Rate Data," *IEEE Transactions on Aerospace and Electronic Systems*, Vol. 48, No. 3, 2012, pp. 2628–2637, 10.1109/TAES.2012.6237613.

[14] A. Wittig, P. Di Lizia, R. Armellin, K. Makino, F. Bernelli Zazzera, and M. Berz, "Propagation of large uncertainty sets in orbital dynamics by Automatic Domain Splitting," *Celestial Mechanics and Dynamical Astronomy*, Vol. 122, No. 3, 2015, pp. 239–261, 10.1007/s10569-015-9618-3.